ROTI Keograms based on CMONOC to characterize the ionopsheric irregularities in 2014

Jinghua Li (jhli@nao.cas.cn)
National Astronomical Observatories Chinese Academy of Sciences https://orcid.org/0000-0001-9917-5879

Guanyi Ma
National Astronomical Observatories Chinese Academy of Sciences

T. Maruyama
National Institute of Information and Communication Technology

Qingtao Wan
National Astronomical Observatories Chinese Academy of Sciences

Jiangtao Fan
National Astronomical Observatories Chinese Academy of Sciences

Jie Zhang
National Astronomical Observatories Chinese Academy of Sciences

Xiaolan Wang
National Astronomical Observatories Chinese Academy of Sciences

Research Article

Keywords: ROTI, ionospheric irregularity, drift velocity, keogram, irregular patch

Posted Date: April 11th, 2022

DOI: https://doi.org/10.21203/rs.3.rs-1509581/v1

Abstract

Ionospheric irregularities have been studied since ~70 years ago. With the development of global navigation satellite system (GNSS), GNSS networks have been used to get the characteristics of the irregularities, including the drift velocity, the structure, and the evolution and so on. In this paper, keograms based on the Crustal Movement Observation Network of China (CMONOC) were used to characterize the irregularities over the area from 85 to 125°E in longitude and 11 to 35°N in latitude in 2014. Keograms were obtained for the rate of TEC index (ROTI) in each 0.5 longitude degrees and 30 minutes universal time pixel. The results showed that the occurrence rate of irregularities was high in the equinox months and December, and lowest in June in 2014. In equinox months the irregularities often appeared after sunset. In March the irregularities usually had long lifetime of ~5-7 hours and ~5 degrees apparent longitude scales. The long lifetime usually was accompanied by obvious eastward drift of ~100m/s and large vROTI. In September the irregularities had weaker ROTI and shorter lifetime than those in March. In June, they appeared ~2-3 hours later than those in equinoxes and drifted westward. And the summer irregularities had weakest ROTI and their latitude was ~30°N, much higher than those in equinoxes. In December, the irregularities had small patches with a longitude scale of ~2 degrees and short lifetime of ~2 hours. Different from the equatorial irregularities in equinox months, the solstice irregularities mainly appeared should be local phenomenon.

1. Introduction

Ionospheric equatorial plasma bubbles (EPBs) or irregularity is an important issue in space weather because it can cause the amplitude and phase fluctuation of the radio signals passing through it, or even degrade the critical radio system performance. It has been widely studied by different techniques such as ionosondes, radars, satellite in-situ measurement, airglow imagers, and Global Navigation Satellite Systems (GNSS) receivers. Regarding the GNSS receivers, observation networks have been constructed, such as international GNSS service (IGS), GNSS Earth Observation Network System (GEONET) of Japan, the Crustal Movement Observation Network of China (CMONOC) and so on. Such networks make it possible to monitor the ionospheric parameters in a large area.

Two important parameters, total electron content (TEC) and rate of TEC index (ROTI), have been widely used to specify the ionosphere and ionospheric irregularities. TEC maps and ROTI maps are provided as products by some regional or global GNSS networks, such as IGS, GEONET and other organizations or institutes to present the background of the ionosphere and the irregularities (Hernández-Pajares et al., 2009; Cherniak et al, 2018). With more and more receivers have been set up by CMONOC, TEC maps and ROTI maps based on CMONOC have been used to study the ionospheric irregularities over China and adjacent regions (Aa et al., 2018; Wei et al., 2020).

Although successive ROTI maps can show the temporal-spatial evolution of the ionospheric irregularities, they cannot present the structure of the irregularities. Some authors gave their methods to obtain the structure of the ionospheric irregularities. Ma et al (2020) proposed a spatial fluctuation of TEC (SFT)

parameter and presented SFT maps to show the spatial structure of the ionospheric irregularities including the size, shape, orientation and intensity distribution of the irregularity structures. A TEC/ROTI keogram, which is a cross section of TEC/ROTI at various times and longitudes or latitudes, can present the drift velocity, the longitude separation distance, and the lifetime of the ionospheric irregularities (Buhari et al., 2014; Diego Barros et al., 2018; de Jesus et al., 2020).

In this study a longitude-time vertical ROTI (vROTI) keogram based on CMONOC is obtained to show the characteristics of the irregularities. A large coverage of the area allowed us to monitor several irregular patches simultaneously from the onset to disappearance over the southern part of China and adjacent regions. The paper is arranged as follows: section 2 describes the data and method to get the keograms. Section 3 is the observation results in 2014. The discussion is processed in section 4. Section 5 summarizes this work.

2. Data And Method

2.1 Date and method to get the vertical ROTI

In this paper, 80 GNSS receivers of CMONOC at the latitude below 30°N were used to study the ionospheric irregularities, as shown in Figure 1. The black dots are the locations of the receivers. The distribution of GNSS receivers covers a longitudinal range of 40 degrees (zonal distance of ~4000km) from ~85°E to 125°E. This is capable of continuously observing the temporal-spatial evolution of the ionospheric irregularities in a large longitude range.

Based on the carrier phase measurement of the GNSS receivers, the slant TEC (sTEC) was calculated every 30s for each receiver-satellite pair (Ma and Maruyama, 2003). To mitigate multipath effects, only data with satellite elevation larger than 30 degrees were used. ROT was determined by taking the difference between the sTECs at two consecutive times. ROTI is defined as the standard deviation of ROT in 5 minutes and it is used to quantify TEC fluctuation (Pi et al., 1997). ROTI can be a measurement of the irregularities with scale-size in order of tens of kilometers. For one GNSS receiver, an irregularity encounter is reckoned if more than 20 consecutive ROTIs are larger than a threshold. The threshold, which could be different for different receivers and was around 0.2 TECU/min, was determined by the sum of the average and 10 times root mean square (RMS) of all ROTIs collected during daytime 6:00 LT to 18:00 LT for a given receiver (Ma et al., 2019). Assuming the ionosphere located in a thin layer at 400 km above the ground, the tracks of the ionospheric piercing point (IPP) can be determined for each satellite-receiver pair. The vROTI, , represented vertical TEC fluctuation and was used to construct ROTI keograms. Where, is the zenith angle of the satellite at IPP.

2.2 Method to get the longitude-time ROTI keogram

After vROTI was calculated for each IPP, ROTI keogram was obtained by binning vROTI into 0.5°×30min longitude-time pixels. The mean vROTI and the percentage of vROTI exceeding the threshold were calculated in each pixel. Figure 2 is an example of the keogram on March 1st 2014. The horizontal axis is

the longitude, and the vertical axis is the universal time. The color map represents the mean vROTI as indicated by the color bar on the right and the white contours are the percentage of vROTI exceeding the threshold. The blue dashed line indicates the E-region sunset time at 20°N.

The figure revealed that the irregularities mainly appeared after E-region sunset. Four major patches can be observed obviously with an apparent longitudinal width of ~5 degrees. The real longitudinal width may be smaller than the apparent width because the inclined patches of irregularity in real space yield a large width of patches in keogram.

Each patch had the lifetime of 5~7 hours. All of the patches did not along the same longitude but tilted eastward. For example the irregular patch at 95°E appeared at ~13:00UT. As time went on, the patch arrived at 103°E at ~16:00UT. This suggested the irregular patch moved eastward. The eastward drift speed can be estimated by the slope of patch. The eastward speed is estimated to be about 103m/s assuming that the irregularities are at 20°N. If the irregular patch is located at 15°N or 25°N, the velocity estimation will be ~106m/s or ~100m/s. Considering that the ionospheric irregularities usually appeared at the low latitude in the equinoxes, the irregularities are assumed to be at 20°N in the speed estimation for simplicity. The four major patches have similar slope, implying that they drift eastward at similar speed. It also can be noted that vROTI became weak during the evolution of each patch until the irregular patch disappeared finally.

It also can be noted that there are some meso-scale structures inside each patch. Previous studies showed that the small-scale ionospheric irregularities usually coexist with large-scale ionospheric irregularities. Owing to the pixel of 0.5 degree by 30 min, irregular patches or structures smaller than ~100 km are obscured on the keograms. The irregularities in March, June, September and December are analyzed in the following sections using the keograms based on CMONOC.

3. Results Based On The Roti Keograms In 2014

3.1 Irregularities in March 2014

The ionospheric irregularities occurred every day in March 2014 as shown in Figure 3. It can be seen that the irregularities had different characteristics day by day in this month. Most of time, the irregularities had several patches between 85°E and 125°E. They appeared successively from east to west owing to different sunset time. From the local time (LT), all of them appeared at ~19:00 LT. On most of days the longitudinal width of the irregular patch is ~5 degree. But the longitudinal gap between two patches is large or small without regular. It can be noted that the longitudinal width of the irregularities is associated to the strength of vROTI. The largest irregular patch was on 68^{th} day when vROTI was large, and on the 79^{th} and 80^{th} day when vRTOI was weak, the irregular patches were small. Figure 3 also showed that there are some small irregular structures in a large patch. For example, the west patch on 61^{st} day included three small structures with large vROTI. For the strongest irregularity on 68^{th} day, the large patch bifurcated into several branches at 14:30~16:00 UT by different vROTI.

On the most days in March, the irregular patches on the keograms tilted eastward as time went on, owning to the eastward drift of the irregularities. The obvious eastward drift usually appeared on the ionospheric irregularities with long lifetime (more than 4 hours) and large vROTI values. On a few days, the irregular patches did not show obvious eastward tilt, for example on the 62nd, 63rd, 77th, 79th, 80th and 86th day of this year. On these days, these irregularities had short lifetime, small longitudinal width and weak vROTI.

For the irregularities with obvious eastward tilt, the eastward speed of the irregularities can be estimated from the longitude-time vROTI keograms. The results were shown in Figure 4. The gaps in this figure owed to no obvious eastward speed from the keograms on these days. The eastward speed usually was about 120m/s, with a range from 90m/s to 160m/s.

3.2 Irregularities in June 2014

Figure 5 is the vROTI keograms in June 2014. Ionospheric irregularities were encountered by CMONOC on eight days in June (the monthly occurrence was 27%). The occurrence time of the irregularities was about 2~3 hours later than 19:00 LT. The irregularities did not drift eastward; inversely they often showed a westward drift in the summer solstice month. The westward drift speed was about 80~130 m/s. The lifetime of the irregularities was about 3~6 hours. Compared with those in March, the irregularities had weaker vROTI and shorter lifetime.

3.3 Irregularities in September 2014

In September, the irregularities observed on the vROTI keograms are shown in Figure 6. There were 24 days on which the irregularities occurred. The monthly occurrence rate of 80% was more than the occurrence rate in June and less than that in March. The occurrence time of the irregularities was often at 19:00 LT. In this month the irregularities only had large spatiotemporal range on several days. The large patches also drifted eastward like those in March. Most of time the irregularities in our observation range consisted of several small patches. Every patch had a lifetime of ~1 hour and longitude range of ~2 degrees. These small patches did not show obvious drift on the vROTI keograms. The strength of vROTI in September was stronger than that in June and weaker than in March.

3.4 Irregularities in December 2014

In December, the irregularities appeared on 15 days with the monthly occurrence rate of 48%. The irregularities in this month were very different from other three months in the range, lifetime and occurrence time. The keograms were shown in Figure 7. On the 335th day the irregularities continued sporadically from 10:00~20:00 UT at the longitude of 115°E. On the 345th day the irregularities continued sporadically in large longitude range. And on 357th and 365th days, only one irregular patch was observed. Although the irregular patches appeared at different time and longitude range, all the patches had similar longitudinal scale of ~2 degrees and lifetime of about 1~2 hours. The irregular patches on the same day were discrete in time and space. They maybe not associate with each other. It also should

be noted that the irregularities in December had stronger vROTI than those in June and September. And they did not show eastward of westward drift.

4. Discussion

The keograms based on CMONOC in 2014 showed that the irregularities had highest monthly occurrence rate in March, as much as 100%, then 80% in September, 48% in December and 27% in June. The high occurrence in both equinoxes and low occurrence in two solstices are consistent with the previous results (Su et al, 2008). It is worth mentioning that the occurrence rate in December was higher than in June. This is rarely reported in Southeast Asia (Li et al., 2021). Vyas and Dayanandan (2011) reported that the occurrences of VHF scintillations at (24.6°N, 73.7°E) showed a clear seasonal behavior with equinoctial maxima followed by winter and a summer minima during both high and low sunspot activity years. The seasonal occurrence rate of the irregularities in this work was consistent with these results. The seasonal characteristics of occurrence rate showed good correspondence with the vertical drift velocities of the ionospheric plasma (Vyas and Dayanandan, 2011; Su et al., 2008).

The keograms in March showed the irregularities had long lifetime. They usually lasted several hours or till early morning. At the same time, eastward drift was observed at a speed of 90-160m/s. Previous results also showed that the typical eastward drift velocity of the ionospheric irregularities is on the order of ~100-200m/s (Valladares et al., 1996; Kinter et al., 2004). Chapagain et al. (2012) pointed that the observed ionospheric irregularities velocity is consistent with the ambient plasma drift velocity. In the nighttime the equatorial F region plasma drifts eastward (Fejer et al., 1991). Chandra et al. (1993) showed VHF scintillations at the station close to the magnetic equator were strong and lasted till early morning in single patch during March-April 1991 in India, however for the station in the anomaly crest region or beyond, scintillations occurred in small patches with periods of no scintillations in between. The long lifetime and large patch in March 2014 are in agreement with the VHF scintillation observed by Chandra et al. at the station close to the magnetic equator. The irregularities in March may be associated with the EPBs. Figure 8 and 9 showed the typical sTEC and ROTI in March and June 2014. sTEC minus some fixed values are presented to show the relative variation in the same scale. The relative change is concerned in studying the ionospheric irregularities. From figure 8, it can be seen that the sTEC suddenly dropped when the satellite encountered an ionospheric irregularity. This is the typical characteristic of the EPBs.

In June, the irregularities with large range had a westward drift at a speed of 80~130 m/s. This was different from the equinox equatorial irregularities. Figure 9 presented the typical sTEC and ROTI in June. The sTEC began to undulate when it encountered the ionospheric irregularities, quite different from the sharp dropping in March. The longitude-time keograms showed some characteristics of the irregularities, but the latitude information is lost. In order to understand the characteristics of the irregularities, the latitude ranges of the irregularities based on the latitude-time keograms are summarized in Figure 10. It showed that the irregularities in June often appeared at ~30°N. The irregularities in June with westward drift may be related to the medium-scale traveling ionospheric disturbances (MSTIDs). And the sTEC

undulation is similar to the pattern of MSTIDs. Previous study pointed that the nighttime MSTIDs are mainly observed in middle latitude and their propagation direction is primarily southwest in the northern hemisphere (Otsuka et al. 2004; Takahashi et al., 2018). They are more active during June solstice and they can propagate to lower latitude (Sivakandan et al., 2019).

In September, the occurrence rate, the lifetime, the ROTI values and the longitude scale of the irregularities were weaker than those in March. The occurrence time and the eastward drift were similar to those in March, different from those in solstice months. Previous study also showed the equinoctial asymmetry in the occurrence, which was greater in the spring equinox than in the autumn equinox. The asymmetry may be attributed to differences in plasma densities and meridional winds during two equinoxes [Nishioka et al., 2008; Maruyama et al., 2009; Otsuka et al., 2006; Sripathi et al., 2011].

In China, the irregularities are rarely reported in December. The GPS scintillation in south of China occurred mainly in the equinox months with particularly low solar activity during winter and summer months (Huang et al., 2014; Deng et al., 2013). The higher occurrence in winter than in summer is different from the previous results. There are two reasons for this phenomenon. The first one is the different latitude. In this work, the latitude ranges of the receivers are below 30°N, higher than those in Huang and Deng's study. Figure 9 also showed the winter irregularities mainly appeared at 20~30°N. Besides higher latitude range, 2014 is the solar maximum year; the occurrence rate in high solar activity year is different from the low and moderate solar activity. Deng et al. (2013) also pointed that the occurrence of GPS scintillation increased in winter months in enhanced solar activity years (January 2011 to March 2012). Some researchers found that the occurrence rate of VHF scintillation or spread F in the low-latitude of Indian peaked in the equinoxes and winter during the high solar activity period; and during the low solar activity period the occurrence peaked in equinoxes and summer (Kumar et al., 2000; Singh et al., 2004; Vyas and Dayanandan, 2011; Sahithi et al., 2019; Swapna et al., 2015). In this work the results were based on the data in high solar activity year 2014, and the winter irregular mainly appeared in low-latitude (20~30°N). Another characteristic of the winter irregularities is patchy and discrete. Vyas and Dayanandan (2011) pointed that patchy and discrete are the features of scintillations over equatorial anomaly region.

5. Summary

Dual-frequency GPS observations from CMONOC were used to analyze the irregularities in 2014 over the south of China. The longitude-time vROTI keograms were obtained by binning the observation range into 0.5°×30min longitude-time grid cells. The longitude width and the drift velocity and the lifetime of the irregularities can be estimated from the keograms. The results showed that the ionospheric irregularities had the highest occurrence of 100% in Mach, then in September, December and the lowest in June. In March the irregularities had an apparent longitudinal scale of ~ 5 degree and most of time they drift eastward at a speed of ~ 100 m/s with a long lifetime of 5 ~ 7 hours. Sometimes, the irregularities just stayed at the same longitude, did not move. Such motionless irregularities had weak ROTI and short duration. The irregularities in September are similar to those in March except weaker ROTI and shorter

lifetime. In the solstice months, the irregularities appeared at higher latitudes than those in equinoxes. They had different characteristics in the two solstice months. In June, the irregularities usually had weak ROTI and drifted westward. But in December they were patchy and discrete with stronger ROTI than those in June and September. The irregularities in the equinox months should be from lower latitudes beyond our observations. The irregularities in the solstice months may be local phenomena. Further studies are needed to understand the features of the irregularities in June and December.

Abbreviations

GNSS: global navigation satellite system

CMONOC: Crustal Movement Observation Network of China

EPBs: equatorial plasma bubbles

IGS: international GNSS service

GEONET: GNSS Earth Observation Network System

TEC: total electron content

ROTI: rate of TEC index

SFT: spatial fluctuation of TEC

vROTI: vertical ROTI

sTEC: slant TEC

RMS: root mean square

IPP: ionospheric piercing point

MSTIDs: medium-scale traveling ionospheric disturbances

Declarations

Ethics approval and consent to participate

Not applicable

Consent for publication

Not applicable

Availability of data and materials

The datasets analyzed in the study are available from https://data.earthquake.cn/index.html by reasonable request.

Competing interests

The authors declare that they have no competing interests..

Funding

This work is funded by the National Natural Science Foundation of China (Grant numbers. 12073049, U2031146 and 11873064).

Authors' contributions

J.L., G.M. and T.M. purposed the conception, investigation and the method.

J.L., J.F. and J.Z. programmed the software to process the data.

X.W. prepared some figures.

J.L., Q.W. prepared the original draft.

G.M. and T.M. reviewed and checked the manuscript.

Acknowledgements

The authors acknowledge the Crustal Movement Observation Network of China (CMONOC) for the data provision.

References

1. Aa E, Huang W, Liu S, Ridley A, Zou S, Shi L, Chen Y, Shen H, Yuan T, Li J, Wang T (2018) Midlatitude plasma bubbles over China and adjacent areas during a magnetic storm on 8 September 2017. Space Weather 16:321–331. https://doi.org/10.1002/2017SW001776
2. Buhari SM, Abdullah M, Hasbi AM, Otsuka Y, Yokoyama T, Nishioka M, Tsugawa T (2014) Continuous generation and two-dimensional structure of equatorial plasma bubbles observed by high-density GPS receivers in Southeast Asia. J Geophys Res Space Physics 119(569–10,580). doi:10.1002/2014JA020433
3. Chandra H, Vyas GD, Rao DRK, Pathan BM, Iype A, Sekaran BRam, Naidu A, Sadique SM, Salgaonkar CS, Tyagi TR, Kumar PN, Vijay S, Lakha, Iyer KN, Pathak KN, Gwal AK, Kumar Sushil, Singh RP, Singh UP, Singh Birbal, Jain VK, Navneeth GN, Koparkar PV, Rao PVS, Rama, Jaychandran PT, Sriram P, Rao NYS, Santa GA, Das BK, Rastogi RG (1993) Coordinated multistation VHF scintillation observations in India during March–April 1991, vol 22. Indian Journal of Radio & Space Physics, pp 69–81

4. Chapagain NP, Taylor MJ, Makela JJ, Duly TM (2012) Equatorial plasma bubble zonal velocity using 630.0 nm airglow observations and plasma drift modeling over Ascension Island. J Geophys Res 117:A06316. doi:10.1029/2012JA017750
5. Cherniak IV, Andrzej Krankowskilrina Z (2018) ROTI Maps, a new IGS ionospheric product characterizing the ionospheric irregularities occurrence. GPS Solutions 22(3). DOI: 10.1007/s10291-018-0730-1
6. Deng B, Huang J, Liu W, Xu J, Huang L (2013) GPS scintillation and TEC depletion near the northern crest of equatorial anomaly over South China. Adv Space Res 51(3):356–365
7. Diego Barros H, Takahashi CM, Wrasse, Cosme Alexandre OB, Figueiredo (2018) Characteristics of equatorial plasma bubbles observed by TEC map based on ground-based GNSS receivers over South America. Ann Geophys 36:91–100. https://doi.org/10.5194/angeo-36-91-2018
8. de Jesus R, Batista IS, Takahashi H, de Paula ER, Barros D, Figueiredo CAOB et al (2020) Morphological features of ionospheric scintillations during high solar activity using GPS observations over the South American sector. J Geophys Research: Space Phys 124. https://doi.org/10.1029/2019JA027441
9. Fejer BG, de Paula ER, Gonzilez SA, Woodman RF (1991) Average Vertical and Zonal F Region Plasma Drift Over Jicamarca. J Geophys Res 96(A8):13901–13906
10. Huang L, Wang J, Jiang Y, Zhao CZh K (2014) A study of GPS ionospheric scintillations observed at Shenzhen. Adv Space Res 54(11):2208–2217
11. Hernández-Pajares M, Juan JM, Sanz J, Orus R, Garcia-Rigo A, Feltens J, Komjathy A, Schaer SC, Krankowski A (2009) The IGS VTEC maps: a reliable source of ionospheric information since 1998. J Geod 83:263–275. DOI 10.1007/s00190-008-0266-1
12. Kintner P, Ledvina B, de Paula E, Kantor I (2004) Size, shape, orientation, speed, and duration of GPS equatorial anomaly scintillations, Radio Sci., 39(2), RS2012
13. Kumar Sushil, Gwal AK (2000) VHF ionospheric scintillations near the equatorial anomaly crest: solar and magnetic activity effects. J Atmos Solar Terr Phys 62:157–167
14. Li G, Ning B, Otsuka Y, Abdu MA, Abadi P, Liu Z, Spogli L, Wan W (2021) Challenges to Equatorial Plasma Bubble and Ionospheric Scintillation ShortTerm Forecasting and Future Aspects in East and Southeast Asia. Surv Geophys 42:201–238. https://doi.org/10.1007/s10712-020-09613-5
15. Ma G, Hocke K, Li. J, Wan Q, Lu W, Fu W (2019) GNSS Ionosphere Sounding of Equatorial Plasma Bubbles, Atmosphere. 10: 676, doi:10.3390/atmos10110676
16. Ma G, Li Q, Li J, Wan Q, Fan J, Wang X, Maruyama T, Zhang J (2020) A study of ionospheric irregularities with spatial fluctuation of TEC. J Atmos Solar Terr Phys 211:105485
17. Ma G, Maruyama T (2003) Derivation of TEC and estimation of instrumental biases from GEONET in Japan. Ann Geophys 21(10):2083–2093
18. Maruyama T, Saito S, Kawamura M, Nozaki K, Krall J, Huba JD (2009) Equinoctial asymmetry of a low-latitude ionosphere-thermosphere system and equatorial irregularities: evidence for meridional wind control. Ann Geophys 27:2027–2034

19. Nishioka M, Saito A, Tsugawa T (2008) Occurrence characteristics of plasma bubble derived from global ground-based GPS receiver networks. J Geophys Res 113:A05301
20. Otsuka Y, Shiokawa K, Ogawa T, Yokoyama T, Yamamoto M, Fukao S (2004) Spatial relationship of equatorial plasma bubbles and field-aligned irregularities observed with an all-sky airglow imager and the Equatorial Atmosphere Radar. Geophys Res Lett 31(20):L20802
21. OTSUKA Y, SHIOKAWA K, OGAWA T (2006) Equatorial ionospheric scintillations and zonal irregularity drifts observed with closely-spaced GPS receivers in Indonesia. J Meteorol Soc Jpn 84A:343–351
22. Pi X, Mannucci AJ, Lindqwister UJ, Ho CM (1997) Monitoring of global ionospheric irregularities using the worldwide GPS network. Geophys Res Lett 24:2283–2286
23. Sahithi K, Sridhar M, Sarat K, Kotamraju KCh, Sri Kavya G, Sivavaraprasad DVenkata, Ratnam ChD (2019) Characteristics of ionospheric scintillation climatology over Indian low-latitude region during the 24th solar maximum period, Geodesy and Geodynamics, Volume: 10, Issue: 2, 110–117, DOI: 10.1016/J.GEOG.2018.11.006
24. Singh RP, Patel RP, Singh AK (2004) Effect of solar and magnetic activity on VHF scintillations near the equatorial anomaly crest. Ann Geophys 22:2849–2860. DOI: 10.5194/angeo-22-2849-2004
25. Sivakandan M, Chakrabarty D, Ramkumar TK, Guharay A, Taori A, Parihar N (2019) Evidence for deep ingression of the midlatitude MSTID into as low as ~ 3.5° magnetic latitude. J Geophys Research: SpacePhysics 124:749–764. https://doi.org/10.1029/2018JA026103
26. Sripathi S, Kakad B, Bhattacharyya A (2011) Study of equinoctial asymmetry in the Equatorial Spread F (ESF)irregularities over Indian region using multi-instrument observations in the descending phase of solar cycle 23. J Geophys Res 116:A11302. doi:10.1029/2011JA016625
27. Su S-Y, Chao CK, Liu CH (2008) On monthly/seasonal/longitudinal variations of equatorial irregularity occurrences and their relationship with the post sunset vertical drift velocities. J Geophys Res 113:A05307. doi:10.1029/2007JA012809
28. Swapna Raghunath, Venkata Ratnam D (2015) Detection of Low-Latitude Ionospheric Irregularities From GNSS Observation, IEEE JOURNAL OF SELECTED TOPICS IN APPLIED EARTH OBSERVATIONS AND REMOTE SENSING. 8:5171–517611
29. Takahashi H, Wrasse CM, Figueiredo C, Barros D, Abdu MA, Otsuka Y, Shiokawa K (2018) Equatorial plasma bubble seeding by MSTIDs in the ionosphere. Progress in Earth and Planetary Science 5:32. https://doi.org/10.1186/s40645-018-0189-2
30. Valladares CE, Sheehan R, Basu S, Kuenzler H, Espinoza J (1996) The multi-instrumented studies of equatorial thermosphere aeronomy scintillation system: Climatology of zonal drifts. J Geophys Res 101:26839–26850
31. Vyas BM, Dayanandan B (2011) Nighttime VHF ionospheric scintillation characteristics near the crest of Appleton anomaly station Udaipur (24.6°N, 73.7°E). Indian J Radio Space Phys 40:191
32. Wei G, Huang W, Liu G, Aa E, Liu S, Chen Y, Luo B (2020) Generation of ionospheric scintillation maps over Southern China based on Kriging method. Adv Space Res 65(12):2808–2820

Figures

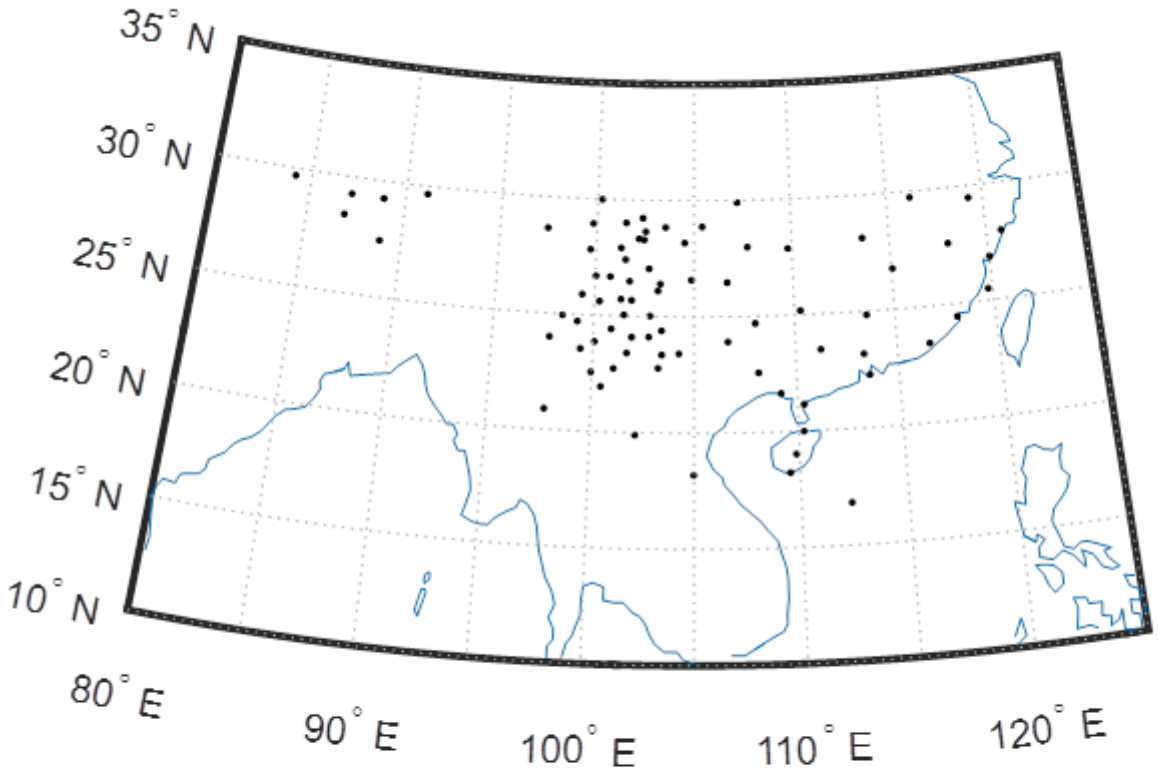

Figure 1 Distribution of the GNSS receiver from CMONOC

Figure 1

See image above for figure legend.

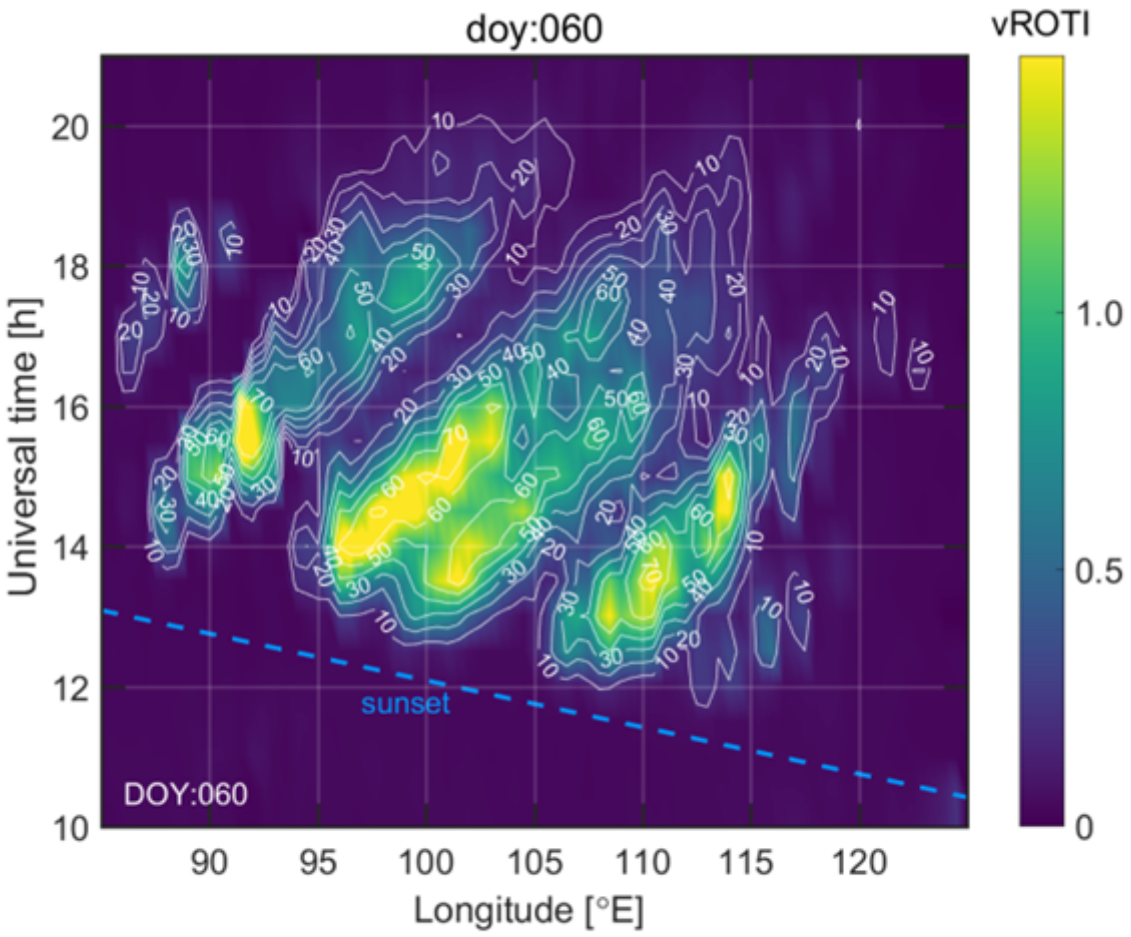

Figure 2. vROTI keogam on March 1st 2014

Figure 2

See image above for figure legend.

Figure 3

See image above for figure legend.

Figure 4

See image above for figure legend.

Figure 5

See image above for figure legend.

Figure 6

Figure 7

See image above for figure legend.

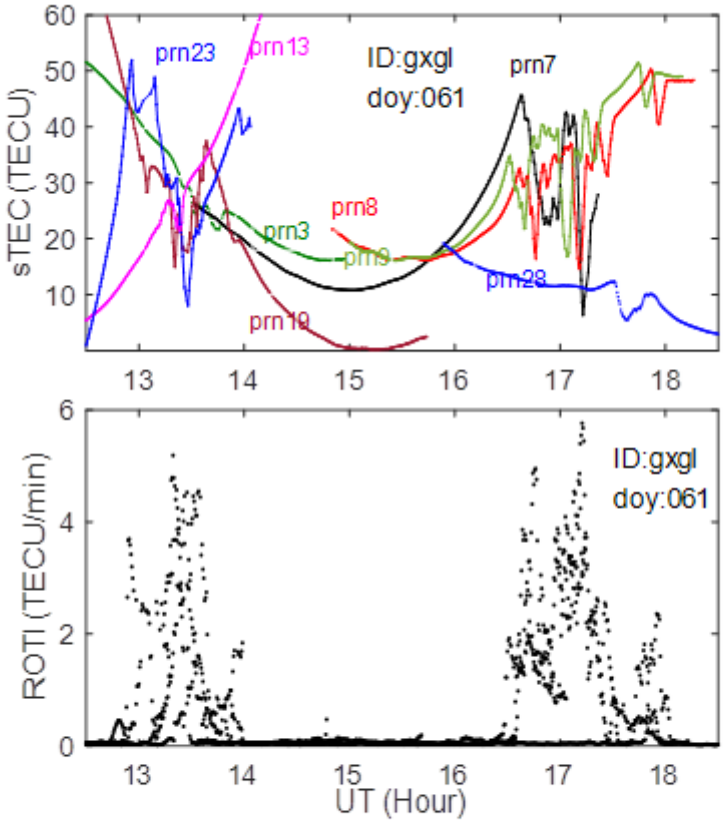

Figure 8 Typical sTEC and ROTI in March 2014

Figure 8

See image above for figure legend.

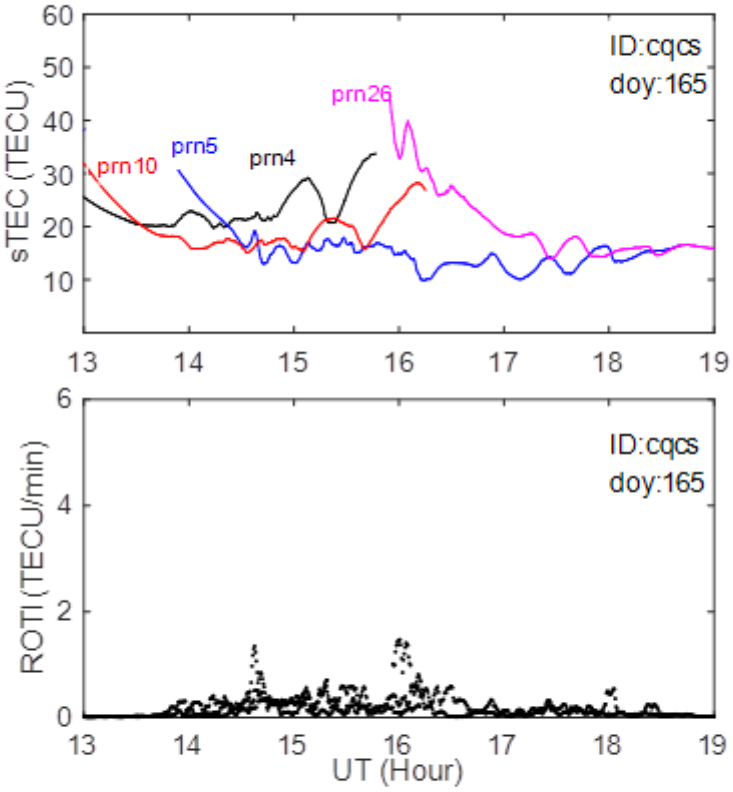

Figure 9 Typical sTEC and ROTI in June 2014

Figure 9

See image above for figure legend.

Supplementary Files

This is a list of supplementary files associated with this preprint. Click to download.

- graphicalabstract.png